

# Boat Dynamics and Force Rendering Models for the SPRINT System

Alessandro Filippeschi, *Member, IEEE*, and Emanuele Ruffaldi, *Member, IEEE*

**Abstract**—The skills professional rowing indoor training (SPRINT) system is designed to support rowing training. The system includes a configurable instrumented rowing apparatus that supports sculling and sweep rowing and that is coupled with a virtual reality display and haptic feedback. Herein, the system has been updated with models that aim at improving force rendering and at simulating the rowing dynamics. These new models support the rendering of vertical and horizontal forces on the hands and they estimate the effects that actions performed on SPRINT would produce on an actual rowing shell. A proof of concept evaluation with one expert and one intermediate rower included a comparison of data gathered on an actual boat and with SPRINT. Outputs of the boat dynamics model showed to be consistent when compared both with the literature and on-boat data. Moreover, these preliminary data suggest boat dynamics output to be useful to discriminate expertise. In addition, subjective ratings of kinematic features and force rendering by expert and intermediate rowers indicated that they find SPRINT suitable for training.

**Index Terms**—Biomechanic modeling, human capturing, multimodal, rowing.

## I. INTRODUCTION

TRAINING in sports is a complex topic which comprises many aspects of human behavior. Fundamental issues for training are the assessment of trainee's performance and the effective and stable transfer of skills to the trainee. Coaches and athletes are required to address these issues to obtain the best results. Therefore, training devices should not only simulate the task in a realistic fashion, but should realize a *training loop* in which trainees can carry out the task without confounding elements (i.e., inconsistency of the task simulation), their performance data are captured and analyzed and feedback is provided.

Within the SKILLS European project [1], a methodology for training was developed: experts' performances were captured and analyzed in order to obtain a digital representation of their skills. This representation was then exploited to develop multimodal interfaces that are able to transfer such skills from the experts to the trainees. Rowing was chosen as a case study for sport training as it requires many motor and cognitive skills. Among

Manuscript received April 30, 2013; revised August 12, 2013; accepted September 23, 2013. Date of publication November 7, 2013; date of current version November 26, 2013. This work was supported by the European SKILLS Integrated Project (IST-FP6 035005). This paper was recommended by Associate Editor A. Karniel of the former IEEE Transactions on Systems, Man and Cybernetics, Part A: Systems and Humans (2012 Impact Factor: 2.183).

The authors are with the PERCRO, Scuola Superiore S. Anna, 33 Pisa, Italy (e-mail: a.filippeschi@sss.up.it; e.ruffaldi@sss.up.it).

This paper has supplementary downloadable multimedia material available at <http://ieeexplore.ieee.org> provided by the authors. This includes a Video of the SPRINT system while being used in the 3D Virtual Environment. This material is 19 MB in size.

Digital Object Identifier 10.1109/TSMC.2013.2284495



Fig. 1. SPRINT system in the immersive setup.

the skills that are required to become an elite rower, current training protocols mostly aim at conditioning the physiological ones, whereas technique and team coordination skills are qualitatively assessed by inspection during training sessions or by means of videotapes analyses carried out long after the performance. Skills Professional Rowing Indoor Training (SPRINT) system (see [2]–[5]), shown in Fig. 1, now includes the collection and processing of real-time information about the trainee's performance that is used to provide training feedback effective for accelerating the learning of motor skills [6], [7] via Virtual Environments [8], [9]

This paper focuses on the force rendering to the user (in particular the vertical force rendering) and the task modeling (i.e., the prediction of boat behavior based on the SPRINT input), including forces and moments on the rower.

After a short summary of rowing bases, the state of the art of the main aspects that deal with rowing simulation and SPRINT are presented. Then, the paper focuses on the models that were developed to improve the force rendering and the simulation of boat's dynamics. The results of the experiments carried out to assess the force rendering and the boat's model are then presented and discussed.

## II. RELATED WORK

### A. Rowing Bases and Current Simulators

Rowing is an outdoor sport in which one or more rowers drive a boat through the water. A rower's interfaces with the boat are the foot stretcher, the sliding seat and one or two oars, respectively, for *sweep rowing* and for *sculling*. Fig. 2 shows a race boat along with the main components. The rower repeats cyclically the same sequence of movements, called *stroke*, which, in turn, can be segmented into four phases. The blades immersion is called the *entry* phase. The *drive* phase comprises leg and

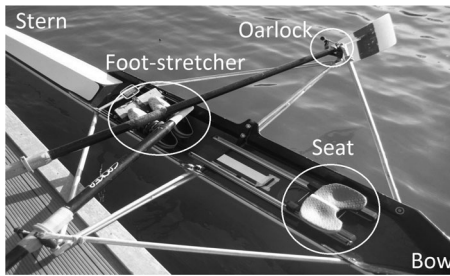


Fig. 2. Rowing single scull.

back action for the propulsion of the boat. When the rower's arms start pulling the *finish* phase begins. The *recovery* phase includes, when the blades are removed from the water and the arms are outstretched. More information about rowing can be found in the FISA handbook [10].

Rowers are often forced by environmental factors to train indoor using rowing simulators. The Gjessing ergometer [11] was the most diffused from its development to late eighties. Since early nineties, the Concept ergometers (Morrisville, VT, USA) were adopted by rowing clubs and federations becoming the international standard for indoor rowing training and rowers evaluation. In both systems, the rower pulls a handle that is connected by a belt or a chain to a device that resists motion. Differently from outdoor rowing, rower forces and motion are in the sagittal plane. Despite this limitation, these simulators are affordable and support rowing training.

Recently, concept-like simulators tried to improve force rendering. For example, in Rowerwater (Warren, RI, USA) resistance is obtained by moving water instead of air, whereas in Rowperfect [12] and in a later version of the concept the platform moves under the rower. This latter solution is closer to outdoor rowing situation, where the hull slides under the rowers which move at an almost constant absolute velocity.

During the last 15 years a new generation of rowing simulators were designed to improve outdoor rowing kinematics and force rendering (e.g., Biorower (Wien, Austria), Oartec Rower (Sydney, Australia)). However, the most advanced ones are in research and development (e.g., ETH M3 rowing simulator [13]). The latter ones exploit data analysis and feedback to enhance realism and training capabilities. However, cost and space limitations detract from marketability.

### B. Rowing Models

Athletes and coaches have always sought methods for evaluating and predicting rowing performance. Physiological variables such as heart rate, lactate, and oxygen uptake are measured and analyzed in order to evaluate rowers and to predict their potential [14]. Biomechanics of rowing is used to evaluate the effectiveness of rowing gesture and to predict boat speed. With respect to rowing dynamics, many models were proposed. In 1925, Alexander [15] modeled the boat and the rower as point masses, and the hydrodynamic forces (due to hull-water and blades-water interaction) proportional to the square of the water-hull relative speed. Alexander considered rower motion to be known and expressed it as a function of time. Other one-dimensional (1-D) models the rower as one or more masses whose displacement depends on either time or oar angle and

forces are calculated (e.g., [16]) or prescribed (e.g., [17]). The simple models of the average hull speed can be found in [18] and [19]. A more complex 1-D model aimed at mimicking recorded data and predicting the hull surge speed [20] accounts for rowers' limbs inertia and considers full kinematics of the rower. Mola's [21] six-degrees-of-freedom (DoFs) model accounts for the water-hull interaction and considers the rower as composed of 12 parts whose masses and motion are prescribed. Mola's model assumes motion and forces to be known (but the model allows for using direct measures of the supposed known variables) and returns hull's motion as result.

### C. SPRINT System

1) *System Components*: This section provides a brief overview of the SPRINT system to contextualize the study shown in this paper.

SPRINT was designed in a modular way to allow for different setups, Fig. 3 shows the SPRINT architecture.

The human interfaces are implemented in the *Mechanics* module, that is designed to support kinematics and force rendering requirements. Fig. 4(a) shows the parts of this module along with the DoFs provided and the regulations available. A frame with two oars and a sliding seat meets the kinematics constraints of outdoor rowing. The design supports differently sized athletes. Switching from sculling to sweep rowing is accomplished by changing the oar (bolted to the frame), adjusting the resistance, and setting the proper regulations. The SPRINT system platform is fixed to the ground and it is different from the outdoor rowing situation. Data (e.g., [14] and [22]) show that the rowers center of mass moves at approximately constant speed, while the hull slides back and forth underneath. To our knowledge, only simulators with simplified kinematics implement sliding platforms (e.g. [12]), whereas a fixed platform has been adopted by more complex simulators (e.g., [13]). For space, only the inboard of the oar is included. In this newer version of SPRINT, a mass-spring system replicates both the oar weight and the hydrostatic vertical forces (see Section III-A). With respect to force rendering, vertical forces are treated in Section III-A. Horizontal forces are due to user-structure interaction from forces that the rower exerts on the hull and the oars. Controlled brakes can accurately replicate the desired load profiles, but they are expensive and require maintenance. Passive air or water-based devices are simpler and do not suffer from overheating, but the force rendering and its regulation are less accurate. The current design includes the Concept2 power dissipation device, that we call PDD, which is composed of a flywheel with a mounted fan. It supports autonomous oar units, but introduces three issues. First, this PDD dissipates all of the rowers work which is more suitable for sweep rowing but not for sculling, where forces are about half for each oar. Second, the fan blades are forward curved; therefore, only one direction of rotation of the PDD is allowed. Third, the oars angular speed is not suitable for the device and needs to be amplified. The first issue was first addressed by providing the PDD with regulation of the air flow. The latter two are solved by introducing a transmission system between the oar and the PDD. It is composed of a bevel gear and a two-stages coaxial planetary gearbox. Bevel gears allows a 90° rotation of the motion axis in order to reduce the overall size of the mechanics, a first transmission ratio of

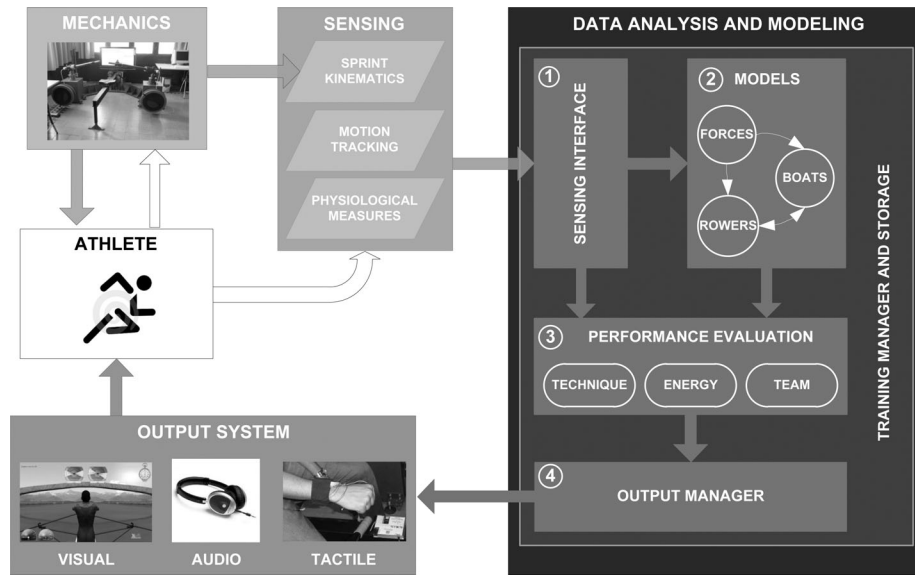


Fig. 3. SPRINT architecture.

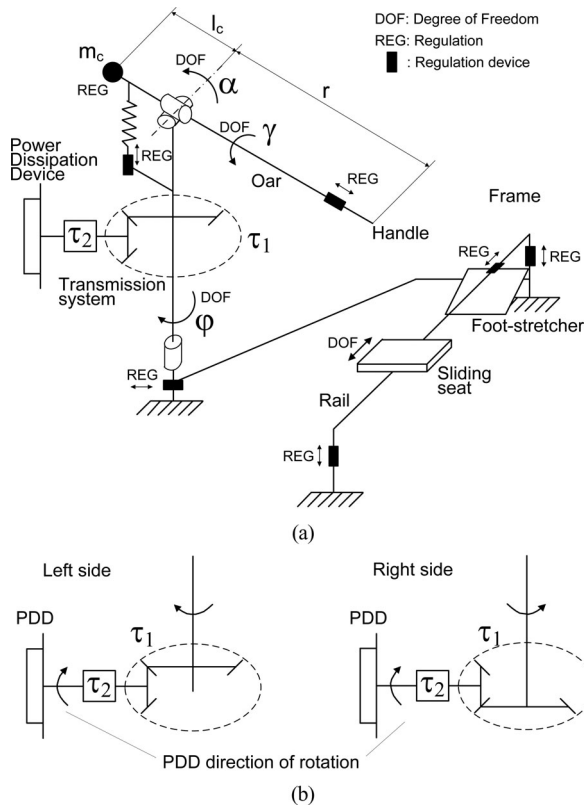


Fig. 4. Mechanics module. (a) Frame connects oar units with the rail. Devices for force rendering (power dissipation device, counterbalance weights, and spring) are represented in the scheme. (b) Transmission system of the SPRINT system. Left and right sides required different setups to use the same PDD. Nomenclature:  $\alpha$ ,  $\varphi$ , and  $\gamma$  are the DoFs of the oar;  $m_c$  is the total mass of the counterbalance weights.  $\tau_1$  and  $\tau_2$  are the transmission ratios of the bevel gear and the planetary gearbox respectively.

$\tau_1 = 4$ , and to adapt the oar’s direction of rotation to the PDD. The planetary gearbox provides a further  $\tau_2 = 16$  transmission ratio in order to solve the third problem [see Fig. 4(b)].

A model of the PDD dynamics was developed and verified to check its usability in SPRINT. It is described in [23] and briefly summarized here. The torque  $C_t$  needed to move the PDD is

$$C_t = C_f + C_i \quad (1)$$

where  $C_f$  and  $C_i$  are the resisting torque due to, respectively, the airflow and the flywheel inertia:

$$C_f = c_q \dot{\theta}^2 + c_v \dot{\theta} + c_c \quad \text{and} \quad C_i = I_{pdd} \ddot{\theta} \quad (2)$$

where  $\theta$  is the PDD’s rotation angle,  $c$  are the coefficients dependent on the geometry (see [23] for details), and  $I_{pdd}$  is the flywheel moment of inertia. The model assumptions (see [23]) make  $C_f$  expression valid for  $\dot{\theta} > 40$  rad/s, that is common PDD operating conditions. How the torque  $C_t$  is related to user’s force  $F$  is described in Section III-B.

The mechanics itself houses some of the sensors composing the *sensing* module, which is made of many devices (see [24] for details). Several sensing setups are available, for the scope of this study we mention the four encoders that capture oars’  $\alpha$  and  $\varphi$  angles [represented in Fig. 4 and formally defined in (23)], the two encoders that read fans’ speeds and an infrared sensor that captures the seat position. The Vicon system (VICON OMG Plc, Oxford, U.K) is integrated with SPRINT to capture shoulders, elbows and wrists positions.

The *Data Analysis and Modeling* module supports the model of the (PDD, models for the rowing simulation, performance evaluation, and feedback. The PDD model provides an estimation of the force exerted by the rower. The boat model estimates hull motion, human-machine interaction forces, and articular loads. Performance analysis addresses technique analysis [3], [25], energy expenditure [4], and team coordination [5]. The training manager, tailored by the rower or the coach, triggers and manages the *feedback* according to the training protocol and the performance analysis. Visual information can be displayed on a screen or projected in a 3-D environment such as a CAVE (CAVE Automatic Virtual Environment) [26]. The boat models are used for driving the boats, the oars, and any virtual teammates or opponents [27]. Raw and processed data, the training

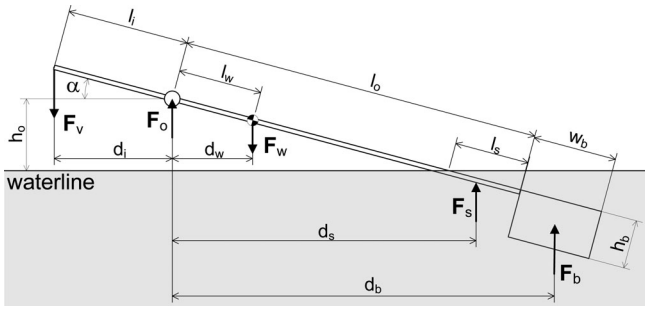


Fig. 5. Scheme and nomenclature for the vertical forces model.  $F_v$ ,  $F_w$ ,  $F_s$  and  $F_b$  are the force on the hand, the oar weight, the hydrostatic force on the immersed oar shaft and the force on the immersed blade respectively.  $l_i$ ,  $l_o$ ,  $l_w$  and  $l_s$  are the oar inboard, the oar outboard, the immersed shaft length and the distance of the oar Center of Gravity (CoG) from the oarlock along the oar respectively.  $d_i$ ,  $d_w$ ,  $d_s$  and  $d_b$  are the distances of  $F_v$ ,  $F_w$ ,  $F_s$ , and  $F_b$  from the oarlock in the water plane.  $h_o$  is the height of the oarlock from the waterline.  $h_b$  and  $w_b$  are the blade height and width respectively.

session procedure, and the feedback activation are recorded and can be retrieved [28].

Vibrotactile, auditory, and visual feedback modalities were studied [29] and are now used. Vibrating motors are mounted on body limbs to convey information about the technique. Both single tones and simulated outdoor rowing noises are auditory cues used for correcting technique faults and for the realism. Haptic feedback is provided by the Mechanics module, discussed next.

2) *Evaluation of the SPRINT System:* Preliminary assessment of the system's training capabilities were carried out by means of several experiments (e.g. [3], [4], [25], and [5]). Those experiments required the first version of SPRINT as it is described in [5], [23], and [24]. This new version of SPRINT focuses on the development of force rendering for outdoor rowing as it is configurable to support both sculling and sweep rowing. The following two sections present models for force rendering and rowing dynamics. Subjective ratings from expert and intermediate rowers and a comparison of rowing data from actual rowing and the SPRINT are used as a proof of concept evaluation of the human-machine interface.

### III. FORCE RENDERING

This section presents the improvements of SPRINT related to vertical and horizontal force rendering.

#### A. Vertical Forces

In steady conditions, vertical forces on the oar depend only on gravity and water hydrostatic force and in working conditions this assumption is not strong (see Appendix A). According to the notation shown in Fig. 5, vertical force perceived on the hand in out-door rowing is

$$F_v = \frac{F_w d_w - F_s d_s - F_b d_b}{d_i}. \quad (3)$$

$F_w$  and  $F_s$  contribution to  $F_v$  depends on the blade and the shaft being immersed. We define  $\alpha_0$  the value of the  $\alpha$  angle when the blade hits the water, and  $\alpha_e$  the correct entry angle. When  $\alpha > \alpha_e$ , the oar shaft is immersed. Given  $l_o$  the oar outboard,

$h_o$  the height of the oarlock from the waterline, and  $h_b$  the blade height (see Fig. 5), we have

$$\alpha_0 = \frac{h_o - h_b}{l_o} \quad \text{and} \quad \alpha_e = \frac{h_o}{l_o}. \quad (4)$$

When  $\alpha < \alpha_0$ , we have  $F_s = F_b = 0$ , this condition sets the correct counterbalance weights. Let now  $l_c$  be the distance between the SPRINT oarlock and the regulation mass  $m_c$  (see Fig. 4), and  $m_i$  be the SPRINT oar mass and  $r$  the SPRINT oar inboard, then  $m_c$  is given by

$$m_c = \frac{F_w l_w - \frac{1}{2} m_i g r}{g l_c}. \quad (5)$$

If  $\alpha \geq \alpha_0$ , hydrostatic forces are

$$F_s = \begin{cases} 0 & \alpha_0 \leq \alpha < \alpha_e \\ \rho_w V_s g & \alpha \geq \alpha_e \end{cases}$$

$$F_b = \begin{cases} \rho_w V_b g \frac{\alpha - \alpha_0}{\alpha_e - \alpha_0} & \alpha_0 \leq \alpha < \alpha_e \\ \rho_w V_b g & \alpha \geq \alpha_e \end{cases}$$

where  $\rho_w$  is the water density,  $V_s$  and  $V_b$  are the shaft's and the blade's immersed volumes, respectively. When  $\alpha > \alpha_e$ , the blade's immersed volume is constant whereas the shaft's has to be calculated. Within the typical ranges of  $\alpha$  the section  $S_s$  of the immersed oar is almost uniform, then

$$V_s = S_s l_s = S_s l_o - \frac{S_s h_o}{\sin \alpha} \quad (6)$$

$l_s$  being the length of the immersed oar shaft.

By putting  $F_w = 0$  in (3), we obtain the contribution of hydrostatic forces [real force line in Fig. 6(c)] to  $F_v$ . It depends linearly on  $\alpha$  when  $\alpha_0 \leq \alpha < \alpha_e$ , it is proportional to  $-\frac{1}{\sin \alpha}$  when  $\alpha > \alpha_e$ . Such a force profile is well approximated by using a spring. Fig. 6 shows the counterbalance weights and the spring that was added to SPRINT along with its contribution to  $F_v$  depending on  $\alpha$ . Fig. 6(c) shows  $F_v$  due to hydrostatic effects (i.e., when  $F_w = 0$ ) in outdoor rowing against  $F_v$  due to the spring force in SPRINT. Such forces are almost equal when  $\alpha_0 < \alpha < \alpha_f$  being equal, when  $\alpha = \alpha_0$ , and when  $\alpha = \alpha_f$ .  $F_v$  due to the spring is greater than hydrostatic forces contribution when  $\alpha > \alpha_f$ . The rendered force is hence bigger than outdoor rowing when blades are immersed too far, i.e., the system provides an amplified feedback when error exceeds  $\alpha_f - \alpha_e$ . Since  $\alpha_f$  depends on the spring setting, rendered force can be adjusted by setting spring's initial position and compression.

#### B. Horizontal Forces

Horizontal forces are provided by the PDD whose dynamics model is recalled in Section II-C1. Given the model of equation (2), the PDD has been assessed on the SPRINT platform with regard to the regulations for the required load ranges for sculling and sweep rowing. Load cells were mounted and calibrated on the shaft of the oarlock to measure horizontal hand force  $F$  thus allowing us to assess transmission system efficiency  $\eta_t$ . Given the PDD torque  $C_t$  [see (1)],  $F$  is estimated as

$$F = \frac{\tau_1 \tau_2 \eta_t C_t}{r} \quad (7)$$

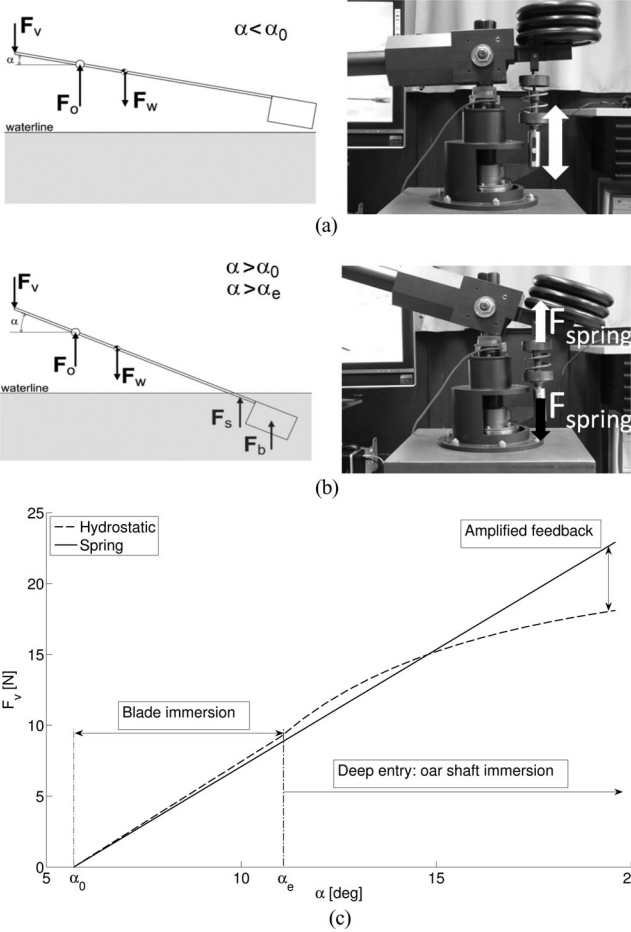


Fig. 6. Vertical forces. (a) Blade is out of the water and the spring is relaxed ( $\alpha < \alpha_0$ ). (b) Deep entry ( $\alpha > \alpha_e$ ), both the blade and the shaft are immersed. (c) Hydrostatic and spring contributions to  $F_v$ , the amplified feedback is reported.  $F_v$ ,  $F_o$ ,  $F_w$ ,  $F_s$ , and  $F_b$  are forces on the handle, from the oarlock, the oar weight, on the shaft, and on the blade.

see Section II-C1 and Fig. 4 for  $\tau_1$ ,  $\tau_2$ , and  $r$  definition. After measuring  $\dot{\theta}$  (i.e.,  $C_t$ ) and  $F$  in different working conditions,  $\eta_t$  was calculated by fitting (7) to have the least-squares error in the most common range of speed ( $\dot{\theta} \in [90, 160]$  rad/s). Once  $\eta_t$  was determined, load cells were not needed anymore to measure  $F$ , that is estimated given PDD speed  $\dot{\theta}$  based on (1) and (7).

Three flywheels are now available for large load's changes, whereas small tuning is obtained by setting the inflow and the outflow of the air in the PDD. These regulations support suitable forces for both sculling and sweep rowing.

#### IV. ROWING DYNAMICS

Three models (hull, oars, and rowers) are merged to create a boat model that estimates boat motion based on users performance on the SPRINT platform. The three are lumped-parameters models, where pressures and volume forces are substituted with specific force-moments equivalent systems. In particular, seat and hand position with respect to the hull as well as forces exerted on the handles are the input for the models. All inertial and geometrical properties are known parameters as they are either measured or taken from tables. The model outputs include hull speed useful for determining the race elapsed

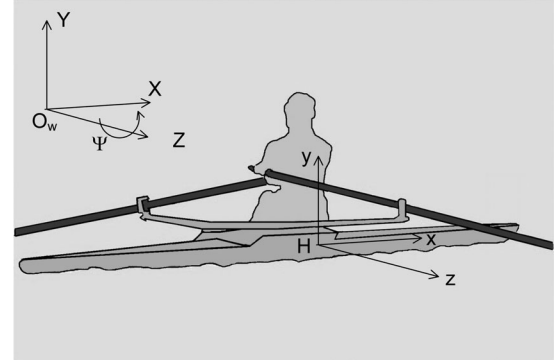


Fig. 7. World and local frames of the boat models. Frame  $(O_w, X, Y, Z)$  is fixed, boat pitch  $\psi$  is also represented. Frame  $(H, x, y, z)$  is attached to the hull, centered in the hull CoG having  $x$  aligned to the seat rail pointing the stern and  $z$  along the oarlocks pointing the left gate.

time. Other important features are the boat secondary motions that can be used to rate technique and to calculate the energy that is wasted without increasing the boat speed. Interaction forces of the rower with the interfaces as well as joint loads are useful to establish whether the effort was exerted in a correct way.

In the following vectors will be written in bold, the magnitude of a vector  $\mathbf{v}_P$  will be written as  $v_P$ , whereas its components with respect to an axis  $i$  will be written as  $v_{P,i}$ . Two orthonormal reference systems are hereby defined along with corresponding unit vectors, the fixed inertial world frame  $(O_w, X, Y, Z)$ , with associated unit vectors  $\mathbf{e}_x, \mathbf{e}_Y, \mathbf{e}_Z$ , and the local frame  $(H, x, y, z)$  with associated unit vectors  $\mathbf{e}_x, \mathbf{e}_y, \mathbf{e}_z$ , both shown in Fig. 7. The former's origin is on the water plane where the  $X$ -axis is horizontal directed toward hull's surge motion and  $Y$  is vertical directed toward the sky. The latter's origin is placed on the boat CoG, its  $x$ -axis is directed toward the stern along the seat rail,  $y$  is directed toward the sky. According to these systems, we define  $\mathbf{p}_I$  is the position of point  $I$  in the  $(O, X, Y, Z)$  system and  $\mathbf{p}_{I,J}$  is the displacement from point  $I$  to point  $J$  in the same system. Similarly,  $\mathbf{p}_i$  and  $\mathbf{p}_{ij}$  are defined for the positions in the  $(H, x, y, z)$  system.

##### A. Hull Model

The boat model considers hull as a 3-DoFs rigid body: the only possible displacement is in the  $(X, Y)$  plane, whereas the only rotation is the pitch  $\psi$  around the  $Z$ -axis. Typically, rowing models account for  $X$  displacement only and they do not consider that immersed volume and wet surface vary with time (hull geometry variability, HGV from now on).

Environmental factors such as wind and waves are not included in the model. Yaw and roll are neglected because the platform is fixed and they cannot be controlled by the user and fed back. In outdoor rowing, yaw is easily controlled by the rower to orient the boat stern in the water plane; moreover, the boat trajectory is straight during a race. Roll is an important component for training because it requires balance and posture control skills and it is not trivial. However, since an haptic feedback would be required to simulate hull's instability, this DoF was neglected both in the platform and in the model. Heave and pitch were kept to provide performance indicators.

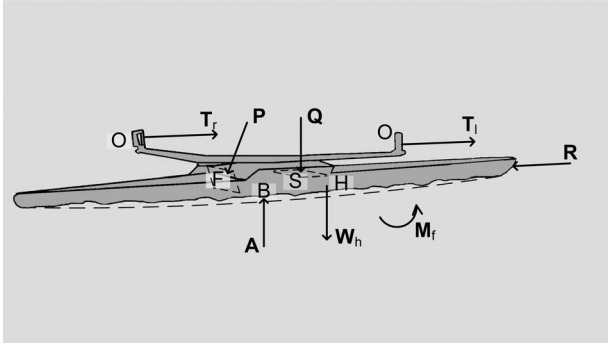


Fig. 8. Free body diagram of the hull. Nomenclature:  $O$ ,  $F$ ,  $S$ ,  $H$ , and  $B$  are points representing the oarlocks, the feet, the seat, the hull CoG, and the hull center of buoyancy, respectively.  $\mathbf{T}_r$  are the forces on the oarlocks,  $\mathbf{P}$  is the force on the foot-stretcher,  $\mathbf{Q}$  is the force on the seat,  $\mathbf{A}$  is the hydrostatic force on the hull,  $\mathbf{W}_h$  is the hull weight,  $\mathbf{R}$  is the resultant drag force on the hull,  $\mathbf{M}_f$  is the resultant pitch moment due to drag actions.

Fig. 8 shows the free body diagram of the hull along with external forces due to the crew, the oars and the water. Momentum balance equations for the hull are

$$\begin{cases} m_h \ddot{\mathbf{p}}_H = \mathbf{T}_r + \mathbf{T}_l + \mathbf{P} + \mathbf{Q} + \mathbf{R} + \mathbf{A} + \mathbf{W}_h \\ I_{H,Z} \ddot{\psi} \mathbf{e}_z = \mathbf{p}_{HF} \times \mathbf{P} + \mathbf{p}_{HO} \times (\mathbf{T}_l + \mathbf{T}_r) \\ \quad + \mathbf{p}_{HS} \times \mathbf{Q} + \mathbf{p}_{HB} \times \mathbf{A} + \mathbf{M}_f \end{cases} \quad (8)$$

where  $H$  is the CoG of the hull,  $B$  is the center of buoyancy of the hull,  $O$  the oarlocks centers,  $F$  the point of the foot-stretcher, where the feet push and  $S$  is the pelvis center. All these points are projected in the  $(X, Y)$  plane. Although  $F$  is steady in SPRINT, as the platform is fixed to the ground, in this model  $F$  moves as the hull does.  $\mathbf{T}$  are the forces oars exert on oarlocks,  $\mathbf{P}$  and  $\mathbf{Q}$  are the forces the rower applies on the foot-stretcher and the seat,  $\mathbf{R}$  and  $\mathbf{M}_f$  are resulting force and moment of drag actions on the hull,  $\mathbf{A}$  is the hydrostatic force due to hull's immersed volume and  $\mathbf{W}_h$  is the hull's weight. Forces  $\mathbf{T}$ ,  $\mathbf{P}$ , and  $\mathbf{Q}$  will be written as part of oars' and rower's balance, whereas forces  $\mathbf{A}$ ,  $\mathbf{R}$ , and moment  $\mathbf{M}_f$ , due to water-hull interaction, are described in the following.

Given water density  $\rho_w$  and hull immersed volume  $V_{imm}$ , hydrostatic force  $\mathbf{A}$  is

$$\mathbf{A} = \rho_w g V_{imm} \mathbf{e}_z. \quad (9)$$

Moment  $\mathbf{M}_{fl}$  of the drag actions was neglected as not relevant with respect to other contributions.

The resultant force  $\mathbf{R}$  was broken down as the sum of four contributions [30]:

$$\mathbf{R} = \mathbf{R}_s + \mathbf{R}_f + \mathbf{R}_w + \mathbf{R}_a. \quad (10)$$

$\mathbf{R}_s$ ,  $\mathbf{R}_f$ ,  $\mathbf{R}_w$ , and  $\mathbf{R}_a$  represent, respectively, skin resistance due the friction of the water flowing on the hull's surface (that is worth 80% of  $R$ ), the form resistance, the force needed for generating waves and the drag force due to the rowers and hull passing through the air. Since the main contribution is from  $\mathbf{R}_s$  (roughly 80%), many models (e.g., [19], [20]) estimated  $\mathbf{R} = k_{ef} \mathbf{R}_s$ , where  $k_{ef}$  accounts for form and wave resistance. Then,  $\mathbf{R}_s$  is estimated as

$$\mathbf{R}_s = C v^2 \quad (11)$$

where  $C$  is constant and  $v$  is defined by (12).

In our approach, a key difference between (10) and (11) is that we take into account that the wet surfaces and immersed volume vary with time, as shown by (13), (15), (17), (18), and (19). Defined

$$v = \dot{\mathbf{p}}_H \mathbf{e}_x \quad (12)$$

the boat speed along  $\mathbf{e}_x$ ,  $\mathbf{R}$  contributions are shown. The skin drag is calculated according to [31]

$$\mathbf{R}_s = \frac{1}{2} \rho_w c_s \Gamma_s v^2 \mathbf{e}_x \quad (13)$$

where  $\Gamma_s$  is the total wet surface of the hull

$$c_s = \frac{0.075}{[\log \text{Re} - 2]^2} \quad \text{and} \quad \text{Re} = \frac{v l_h}{\mu_w} \quad (14)$$

where  $\text{Re}$  is the Reynolds' number,  $l_h$  is the hull's length along  $\mathbf{e}_x$ , and  $\mu_w$  is the dynamical viscosity of the water. The form drag is [19], [32]

$$\mathbf{R}_f = \frac{1}{2} \rho_w c_f \Gamma_s v^2 \mathbf{e}_x \quad (15)$$

where  $c_f$  the form factor value for a rowing hull is

$$c_f = 0.0097(\kappa_{\text{finish}} + \kappa_{\text{entry}}) c_s \approx 0.01 c_s. \quad (16)$$

and  $\kappa$  angles are entry and exit angles (in degrees) measured at the waterline [32]. Wave drag is calculated as [33]

$$\mathbf{R}_w = \frac{1}{2} \rho_w c_w \Gamma_w v^2 \mathbf{e}_x \quad (17)$$

where  $\Gamma_w$  is the square of the beam at the waterline. For a rowing hull, a suitable value for the wave factor is  $c_w = 0.03$ . Finally air drag is [18]

$$\mathbf{R}_a = 0.02 m_v^{\frac{3}{2}} v^2 \mathbf{e}_x. \quad (18)$$

Therefore, (10) can be written as

$$\mathbf{R}(t) = C(t) v^2(t) \mathbf{e}_x \quad (19)$$

where

$$C(t) = \frac{1}{2} \rho_w [c_s(t) \Gamma_s(t) + c_f(t) \Gamma_s(t) + c_w(t) \Gamma_w(t)] + 0.02 m_v^{\frac{3}{2}} \quad (20)$$

and it depends on time.

Since exact calculation of HGV variables  $\chi$ , i.e.,  $V_{imm}$ , the center of buoyancy  $B$  coordinates and the  $\Gamma$  surfaces, would be demanding to be performed online, they were calculated offline as functions of the hull's DoFs. HGV variables are determined by the intersection of the hull and the water plane, that depends on hull's pitch  $\psi$  and heave  $\mathbf{p}_{H,Z}$ .  $\chi$  variables were numerically calculated offline for a wide range of pitch and heave values. The obtained data were fitted with third-order polynomials functions of pitch and heave, thus obtaining, for each HGV variable  $\chi$

$$\chi(\mathbf{p}_{H,Z}, \psi) = \sum_{\substack{i,j=0 \\ i+j \leq 3}}^3 a_{ij} \mathbf{p}_{H,Z}^i \psi^j. \quad (21)$$

These functions are implemented in the Data Analysis and Modeling module and allow for online HGV calculations with a low computation load. Currently, the hull is approximated as

a paraboloid (as it was done in [19]). However, our approach allows for substituting the paraboloid with more refined models of the hull or with data captured from laser scanning of the hull without increasing the online computational load.

Foot, seat, and oarlock position are then written as functions of the hull's DoFs. Defined  $\mathbf{p}_{IJ0}$  as  $\mathbf{p}_{IJ}$  when  $\psi = 0$ , we have

$$\mathbf{p}_{IJ} = R_{Z,\psi} \mathbf{p}_{IJ0} \quad (22)$$

where  $R_{Z,\psi}$  is defined according to Appendix B notation. Since  $\mathbf{p}_{IJ0}$  are the geometrical properties of the boat that are measured during the hull setup, the latter equation reduces geometrical unknown variables to  $\psi$ .

### B. Oars Model

Oar orientations with respect to the hull is represented by the angles  $\alpha$  and  $\varphi$  (see Fig. 4) defined as

$$\alpha = \arcsin(p_{OH_{a,y}}/p_{OH_a}) \quad (23)$$

$$\varphi_{right} = \text{atan2}(p_{OH_{a,x}}, p_{OH_{a,z}}) \quad (24)$$

$$\varphi_{left} = \pi - \text{atan2}(p_{OH_{a,x}}, p_{OH_{a,z}}). \quad (25)$$

Oars are modeled as rigid links. Blade slip and oar inertia are neglected. The first accounts for the energy waste due to blade-water interaction. The latter provides minor contribution (see Appendix A). Oars balance equations are hence

$$\begin{cases} 0 = \mathbf{T} + \mathbf{F} + \mathbf{F}_b \\ 0 = \mathbf{p}_{OH_a} \times \mathbf{F} + \mathbf{p}_{OB_l} \times \mathbf{F}_b. \end{cases} \quad (26)$$

for each oar, where  $Ha$  is the hand and  $Bl$  is the center of the blade. For the resolution of the above equations  $\mathbf{F}$  is supposed to be always horizontal and perpendicular to the oar shaft.  $\mathbf{F}$  is hence defined as a function of the estimated handle force  $F$  and of  $\varphi$ :

$$\mathbf{F} = \begin{bmatrix} F \cos \varphi \\ 0 \\ -F \sin \varphi \end{bmatrix}. \quad (27)$$

Equation (26) then allows for calculating  $\mathbf{T}_l$  and  $\mathbf{T}_r$ .

### C. Rower Model

The model of the rower was developed to estimate both external forces, namely  $\mathbf{P}$  and  $\mathbf{Q}$ , and joint torques. Inertial and geometrical properties of the rower were established according to [34]; such parameters can be either prompted or calculated given rower's height and weight.

The rower interface with the hull and the oars includes handles, seat, and the foot-stretcher (respectively,  $Ha$ ,  $S$ , and  $F$ ) where  $F$  moves with the hull motion. Therefore hand, pelvis, and feet motion is constrained to the oars and hull. The model receives  $F$  and the positions of hands, shoulders, and seat as inputs to calculate in real time  $\mathbf{P}$  and  $\mathbf{Q}$  as well as shoulders, hip, and knee moments, respectively  $M_s$  ( $M_2^1$  in Fig. 10),  $M_h$  ( $M_3^2$  in Fig. 10) and  $M_k$  ( $M_4^3$  in Fig. 10). When shoulders' positions are not available, shoulders are considered to be aligned to the seat along  $\mathbf{e}_y$  at a distance initially set by the user. Fig. 9 shows the kinematic scheme of the rower. This model is made up of two kinematic chains for the lower and the upper body.

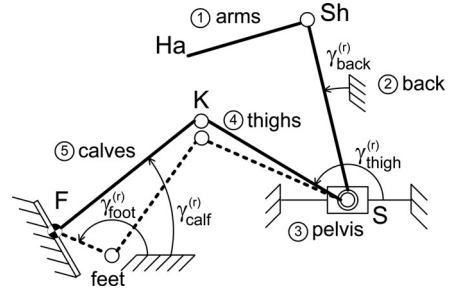


Fig. 9. Rower models kinematics along with nomenclature. The dashed line represent a more realistic model including ankle rotation, and the solid line shows the currently implemented model.

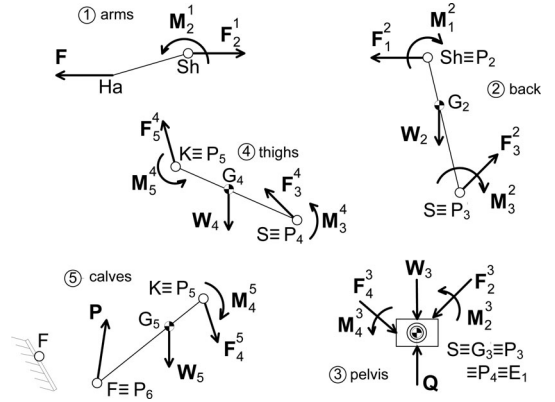


Fig. 10. Free body diagram of the rower.  $G_i$  is the CoG of the  $i$ th body,  $P_i$  the center of the joint connecting  $i - 1$ th and  $i$ th body,  $E_k$  is the  $i$ th body's point, where external force  $\mathbf{F}_k^i$  is applied,  $\mathbf{F}_j^i$  and  $\mathbf{M}_j^i$  are the force and the moment body  $j$ th produces on body  $i$ th.

The first chain is a crank mechanism composed of the pelvis, which only slides, thighs and calves. Whereas ankle rotation is not modeled, displacement of the ankles was taken into account as a variable, dependent on seat displacement, that affects thighs and calves sizes, as shown in Fig. 9. Upper body is composed of the back and the arms, arms inertia is neglected to avoid capturing elbows positions. Fig. 10 shows the free body diagrams for the five bodies. Balance equations for the  $i$ th body are

$$\begin{cases} m_i \ddot{\mathbf{p}}_{G_i} = \mathbf{F}_{i-1}^i + \mathbf{F}_{i+1}^i + \sum_k \mathbf{F}_k^i + \mathbf{W}_i \\ I_i \ddot{\gamma}_i = \left( \mathbf{p}_{G_i P_i} \times \mathbf{F}_{i-1}^i + \mathbf{p}_{G_i P_{i+1}} \times \mathbf{F}_{i+1}^i \right. \\ \left. + \sum_k \mathbf{p}_{G_i E_k} \times \mathbf{F}_k^i + \mathbf{M}_{i-1}^i + \mathbf{M}_{i+1}^i \right) \mathbf{e}_z \end{cases} \quad (28)$$

where  $\ddot{\gamma}_i$  is  $i$ th angular acceleration component along  $\mathbf{e}_z$ ,  $G_i$  is the CoG of the  $i$ th body,  $P_i$  the center of the joint connecting  $i - 1$ th and  $i$ th body,  $E_k$  is the  $i$ th body's point, where external force  $\mathbf{F}_k^i$  is applied,  $\mathbf{F}_j^i$  and  $\mathbf{M}_j^i$  are the force and the moment body  $j$ th produces on body  $i$ th referred to as the connecting joint center. Since  $\mathbf{p}_{HH_a}$ ,  $\mathbf{p}_{HSh}$ , and  $\mathbf{p}_{HS}$  are provided by the sensing module, all geometrical variables of (28) are functions of the captured signals and the hull's DoFs. Once defined angles  $\gamma_i^{(r)}$  (see Fig. 9) for the limbs' orientations in the  $(H, x, y, z)$  frame,

we have

$$\gamma_i = \psi + \gamma_i^{(r)}, \quad \dot{\gamma}_i = \frac{d\gamma_i}{dt} \quad \text{and} \quad \ddot{\gamma}_i = \frac{d\dot{\gamma}_i}{dt}. \quad (29)$$

Equation (30) provides  $\gamma_{\text{thigh}}^{(r)}$  and  $\gamma_{\text{calf}}^{(r)}$ :

$$\begin{cases} (\mathbf{P}_{\text{HS}} - \mathbf{P}_{\text{HF}}) \mathbf{e}_x = l_c \cos \gamma_{\text{calf}}^{(r)} + l_t \cos \gamma_{\text{thigh}}^{(r)} \\ (\mathbf{P}_{\text{HS}} - \mathbf{P}_{\text{HF}}) \mathbf{e}_y = l_c \sin \gamma_{\text{calf}}^{(r)} - l_t \sin \gamma_{\text{thigh}}^{(r)} \end{cases} \quad (30)$$

therefore equation (28) provides a linear system to be solved with the  $\mathbf{F}_{i-1}^i$ ,  $\mathbf{M}_{i-1}^i$ , and  $\mathbf{F}_k^i$  unknowns. The former two are useful for evaluating stress of articulations; the latter two provide  $\mathbf{P}$  and  $\mathbf{Q}$ .

## V. SYSTEM EVALUATION

### A. Methods

Two experiments were carried out to evaluate SPRINT.

In the first experiment, eight rowers (average age 18.37, SD 4.78) with several years of practice (average 7.37, SD 4.44) were asked to row on the SPRINT platform in the two rowing styles (sculling and sweep rowing). Load settings were tuned for sweep rowing. Participants were asked to row at different paces, from the warm-up pace (slow) to race start pace (high). When rowing they were shown the VE and numerical information of the simulated boat speed and of their stroke pace. Then, they were asked to rate the system on a 7-Likert scale composed of 17 items. Here are reported only the seven ones regarding the simulation part:

- 1) the platform allows for rowing as in the common rowing boats;
- 2) the load was too high when sculling;
- 3) the load was too high when sweep rowing;
- 4) I have not enough references to select the oar trajectory;
- 5) the platform is too noisy;
- 6) the platform is too big;
- 7) the simulator is suitable for a rowing club.

In the second experiment, one expert and one intermediate rowers (aged 23 and 28, respectively) rowed on the SPRINT platform, tuned for sculling, and on the instrumented boat. They were asked to carry out the same task and protocol on both platforms: after a calibration and a familiarization phase, they were asked to row for 1 min at low stroke pace (21 spm) and at high pace (30 spm). Both rowers were asked to focus on technique accuracy rather than on the boat speed. On-water data were gathered by means of a single scull provided with sensors and an embedded PC for storage and power supply. Oars angles, seat displacement, as well as hull speed were captured in order to evaluate rower performance.

Hull speed and rower-interface interaction forces were considered, in particular when varying participant's expertise and strokes pace. Overall values of the selected variables were checked to be consistent and, for each variable  $y$ , a regularity score  $\lambda(y)$  was calculated. Given a time dependent variable  $y(t)$  (e.g., hull's speed over several strokes), it is first segmented by stroke. Then, each stroke is decomposed in a suitable fixed number  $n$  of bins. Corresponding bins from different strokes compose a cluster  $Y_i$  with  $i$  in  $1, \dots, n$ , each containing several samples belonging to different strokes. For example, if  $y$  is a

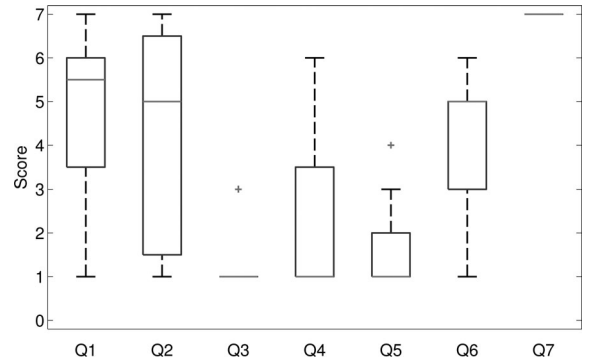


Fig. 11. Boxplots of the rowers' answers.

recording of the hull's speed  $y(t)$  over 15 strokes sampled at 100 Hz and each stroke is divided into 100 clusters,  $y$  will be represented by the set of 100 clusters  $Y_i$ , each one composed of 15 by 10 samples. This operation allow us to represent the sampled  $y$  in the rowing cycle domain (i.e.,  $Y_i$ ) rather than in the time domain (i.e.,  $y(t)$  as it is captured), to support stroke comparison. Since  $Y_i$  is a set of samples (whereas  $y(t)$  is a number or at most a vector), a synthesis of the clusters  $Y_i$  is required to compare rower performances. Since regularity was sought out of data, the coefficient of variation (CV) of each cluster was calculated as

$$z_i = \frac{\sigma_{Y_i}}{\bar{Y}_i} \quad (31)$$

where  $\sigma_{Y_i}$  and  $\bar{Y}_i$  are the standard deviation and the mean of  $Y_i$ . Finally, the regularity index for  $y$  was defined as

$$\lambda(y) = \bar{z}, \quad \text{where } z = [z_1, \dots, z_n] \quad (32)$$

that is the average of the CV over the the whole rowing cycle.

### B. Results

1) *First Experiment Questionnaire:* Fig. 11 shows the boxplots of the answers. Score 1 means that the participant totally disagrees with the statement, whereas 7 means the participant totally agrees with the sentence.

All rowers but one stated that the platform allows for rowing as outdoors, that is the simulator is considered to replicate outdoor rowing. The load in sculling was perceived as too heavy, as was expected because the system was configured for sweep rowing. The third question reveals the value of the load setting. Although some features available in outdoor rowing were missing (e.g., the rigger), rowers did not miss references (except one) to select the oar trajectory. The latter questions were more related to the comfort and the usability of the system. The platform was not perceived as noisy, whereas it was considered too big. Finally, all the rowers agreed that the platform is suitable for a rowing training club.

2) *Boat Model Assessment From the Second Experiment:* We present qualitatively the output of the model itself, then we show a comparison of the SPRINT's output with outdoor rowing data.

The qualitative description of the model output concerns first hull motion, then forces and moments. With respect to hull motion, Fig. 12 shows hull's surge speed along with hull's surge

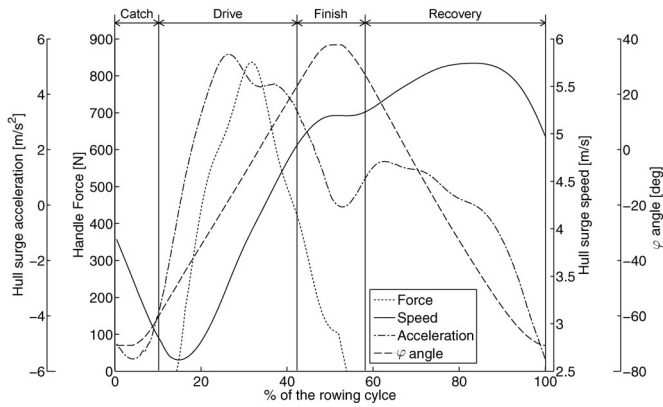


Fig. 12. One stroke performed by an expert rower rowing at 30 spm on the SPRINT platform.

acceleration, force on the handle  $F$ , and  $\varphi$  angle. Data are from one stroke performed by the expert rowing at high pace. At *catch* the rower is switching direction of motion thus accelerating in the  $e_x$  positive direction. This causes the hull to be pushed in the opposite direction. At the same time forces exerted on the handles are still small. Therefore, boat speed decreases in this phase and acceleration reaches its minimum. Then, rower acceleration decreases during the *drive* phase, whereas forces on the handles increase. In this phase, the hull acceleration is maximum and the boat speed quickly increases. During the *drive* resistant force  $R$  increases with the hull speed. At the same time leg action decrease is aided by the back push; then, total force  $F$  drops toward zero as the *finish* phase approaches and only arms propel the boat. Therefore, from the *drive* beginning boat acceleration decreases and it is almost zero at the *finish*, thus explaining the speed peak at the end of the drive. After the *finish* only the rower's inertia and friction act and acceleration turns either negative or positive depending on the balance of such forces. In this phase, rowers have the chance to manage their *recovery* in order to optimize hull speed profile. At high pace inertia usually overtakes friction and a second peak of hull speed happens at half of the recovery phase (e.g., see 80% of the rowing cycle of Fig. 12). At low pace inertia balances friction, hence the hull speed is almost constant during recovery.

We focus now on the foot-stretcher force  $P$ , on the seat force  $Q$ , and on the knee, hips, and shoulders moments. Fig. 13 shows foot-stretcher force on the rower, in particular the component along surge direction (that is  $P_x$ ) during the rowing cycle for an intermediate and an expert rowers. At the catch  $P_x$  is positive (thus decelerating the hull); in this phase pressure on the foot-stretcher makes the rower accelerate in the surge direction. After the catch, the rower's acceleration decreases, but  $P_x$  increases to balance force on the oars' handles. Then, during the late drive and the finish phase,  $P_x$  decreases as  $F$  does. When blades are pulled out from the water  $P$  is determined only by the rower's inertia; hence,  $P_x$  is negative during recovery as the rower moves toward the stern. Fig. 14 shows foot-stretcher and seat forces ( $P_y$  and  $Q_y$ ) for an intermediate and an expert rowers. During the first part of the recovery phase vertical force on the foot-stretcher is almost zero and the rower's weight is totally borne by the seat. As the rower approaches the catch position, vertical force on the foot-stretcher increases; at the same time the load on the seat is

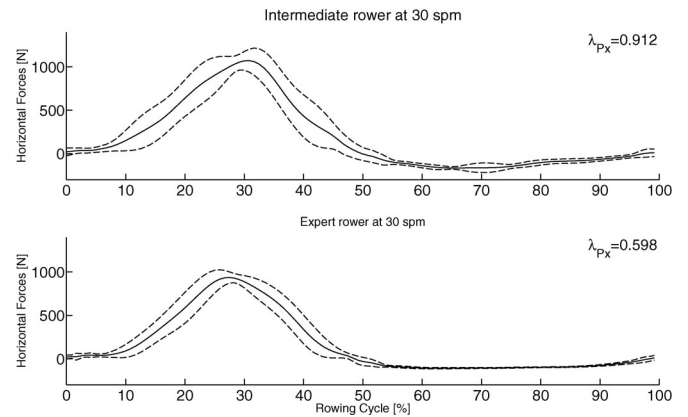


Fig. 13. Average of horizontal force  $P_x$  along with one STD band around average for an intermediate and an expert rowers.

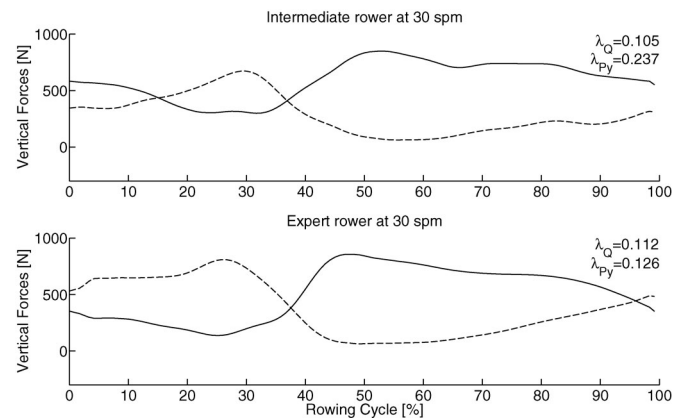


Fig. 14. Average of  $P_y$  (shown by the dashed line) and  $Q_y$  (shown by the solid line) forces for an intermediate and an expert rowers.

reduced. At the catch, rowers start pushing with their legs with  $P_y$  increasing and  $Q_y$  decreasing. During the drive phase,  $P_y$  is still at its highest values. In this phase, the rower has to behave as a kinetic chain that conveys forces between the foot-stretcher and the oars, this behavior is typically considered a correct technique indicator. From this point of view, Fig. 14 shows the expert rower to be more skilled than the intermediate one as, for the expert rower,  $P_y$  is greater than  $Q_y$  beginning at the catch and throughout the drive phase. Conversely, the intermediate rower does not reduce the load on the seat as much and for as much time as the expert rower does. Finally, we report model estimation of shoulders, hip, and knee loads (respectively,  $M_s$ ,  $M_h$ , and  $M_k$ ) that are shown in Fig. 15.

Fig. 16 shows average profiles of boat speed for different pace, device, and expertise conditions. Pace influences drag and inertial forces balance during recovery: at low pace speed is generally lower than at high pace, hence friction, roughly proportional to surge speed square, is lower as well. Nonetheless surge speed is almost constant, thus meaning small acceleration of the rower. Instead, at high pace, surge speed has a second speed peak in the late recovery, that is larger acceleration of the rower. Therefore, these rowers manage differently their inertia depending on pace and this difference is correctly tracked by the system.

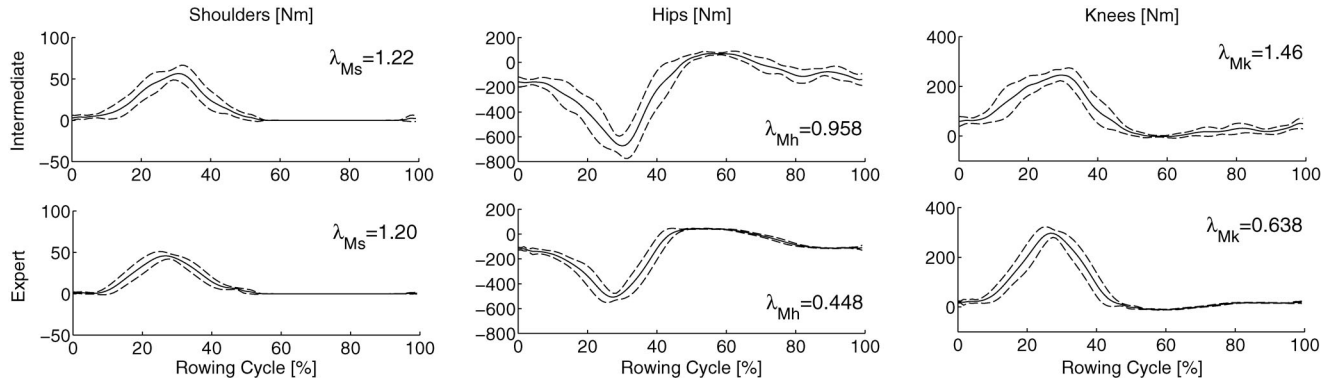


Fig. 15. Average of  $M_s$ ,  $M_h$ , and  $M_k$  along with one STD band around averages for an expert rower and an intermediate rower rowing at high pace.

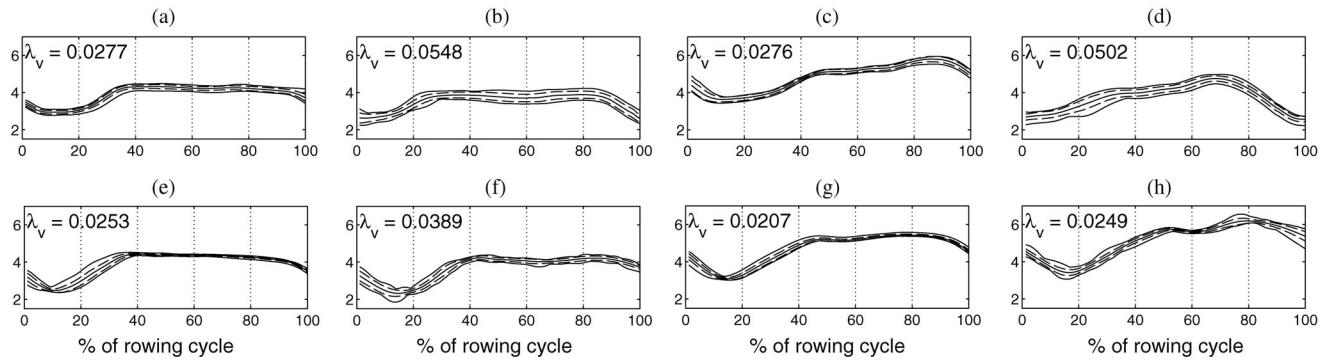


Fig. 16. Average of hull surge speed along with one STD band around average and minimum and maximum speed bands. All expertise, device, and pace conditions are reported. Stroke phases are approximately as follows: catch 0–10%, drive 10–45%, finish 45–55%. (a) On–water Expert low pace. (b) On–water Intermediate low pace. (c) On–water Expert high pace. (d) On–water Intermediate high pace. (e) SPRINT Expert low pace. (f) SPRINT Intermediate low pace. (g) SPRINT Expert high pace. (h) SPRINT Intermediate high pace.

Focusing now on expertise, we see that hull dynamics key features of an intermediate rower are similar to the expert's ones, but intermediate rower's performance is less regular than expert's. Fig. 16 includes  $\lambda_v$  for each condition. As expected, intermediate rower's variability is bigger than expert rower's one regardless the pace and the device.

## VI. DISCUSSION

Evaluation involved both an overall assessment of SPRINT and a specific assessment of the boat dynamics models.

Results of the questionnaire generally suggest a positive feeling of expert and intermediate rowers toward this new system both for how it simulates outdoor rowing and as a training tool. The intensive use of the Concept2 ergometer is a factor that must be taken into account when analyzing these results: answers to questions 2, 3, 5, and 6 indeed may have been influenced by this comparison. SPRINT was not found to be too noisy despite the PDD noise, this answers reveal that the mechanics noise is not disturbing when compared with actual Concept2 PDD's. Conversely, SPRINT was found quite big (it is almost the same length of Concept2 ergometer, but it is much larger, 1.8 m against 0.6 m). Although SPRINT and the Concept2 ergometer have a different kinematics, in particular in case of sweep rowing (that is not symmetrical), the answers about load seem influenced by the comparison with Concept2 ergometer. No rowers indeed had doubts about the correctness of sweep rowing load, even if it is promising for the goodness of the haptic feedback, we must

consider that in case of sweep rowing the load perceived is the same of the Concept2 ergometer. According to sweep rowing answers, it was expected that rowers found load too heavy when sculling, but question 2 answers were not so sharp: most of the rowers found load too high, but for some it was not. We finally report that, although questions 2 and 3 do not clarify whether the load was too low, any rower reported it. In the second experiment rowers tuned load and stated it was good for sculling. Moreover, a qualitative comparison of SPRINT force profiles and force profiles retrieved from the literature, obtained in both on-boat tests (e.g., [35]) and tests on the Concept2 ergometer (e.g., [36]), show that the force rendered by the system is suitable for rowing training.

Vertical force rendering is also important to simulate outdoor rowing, and it is critical when refining rowing technique. The spring mechanism supports correctly vertical force rendering. As the assumptions of the vertical force model are not strong within the common range of oar speed, we did not carry out specific validation activities. Anyway, rowers of the second experiment were asked before and after the experiment and they found vertical force to be suitably simulated once tuned the spring.

The boat dynamics models rely on several assumptions that required a direct comparison with on-boat data to assess the correctness of the results. The ideal validation process would require to provide the SPRINT platform and outdoor rowing boat with the same input, that is the same athletes exerting exactly the same performance with the same environmental conditions.

It is not possible for several reasons: first, SPRINT indeed does not have all the features of a rowing boat moving on the water. Second, environmental conditions (e.g., water stream, wind, and waves) of two trials are not the same. Third, if even these differences were negligible, athletes can not carry out twice the same performance. This is why most of the validation processes of other known models are qualitative, or the models themselves aim at mimicking outdoor rowing captured data. The last solution is good for the model accuracy, but it is detrimental for its usability, as it requires users to perform outdoor rowing session to calibrate the system.

Hull motion output, qualitatively described in Section V-B2, presents the features that are expected and is sensitive to pace variations. The obtained results are consistent with hull speed profiles that we found in the literature (e.g. [14], [22], and [20]). The models of the rower and of the oars rely also on some assumptions. For example, a more realistic model of lower limbs should include the rotational DoF of the ankle, that was considered only indirectly, by changing the calf's length according to the seat position to reduce the problem dimensionality and simplify the requirements for sensing. Forces on the interfaces and articular loads results suggest that these assumptions are not detrimental for the estimation. Estimated forces and articular loads are indeed in accordance with measurements reported in [36] (see Figs. 2 and 3), except for the hips and knee moments. Since the experiment reported in [36] was carried out on a Concept2 ergometer, the difference may be due to the hands height with respect to knees and hips.

Focusing now on expertise, the model output provides some features of skilled behavior (e.g., from  $\mathbf{P}_x$  profiles) that are promising for scoring the user expertise. In particular, the regularity indices always discriminated expertise in the presented examples. On-water performance variability is larger than with SPRINT because of hull stability, waves and other factors that affect performance. However, the index appears to be sensitive enough to distinguish intermediate and expert performance regardless the device, thus being promising for intermediate rowers training. Although we did not run a sufficient number of subjects for concluding  $\lambda$  values to be expertise scores, this proof of concept validation promotes further analysis of such indices.

## VII. CONCLUSION

This paper presented the models and the mechanical solutions aimed at improving the SPRINT system. Models for force rendering supported suitable force rendering in the usual operating conditions especially thanks to the regulations they are provided with. The model of the boat has given consistent and stable results regarding hull's motion, forces on the interfaces, and rower's inner forces. Moreover, these models have revealed to be promising to provide features that aimed at distinguishing experts and intermediate rowers, thus being suitable for high level training. This study is the basis for an enhancement of the rowers performance evaluation based on rowing dynamics. Since our final goal is to assess SPRINT training capabilities, a deeper knowledge of rowers performance outcome will allow us to enhance the training evaluation activities presented in the works cited in Sections I and in II for both novice and intermediate rowers.

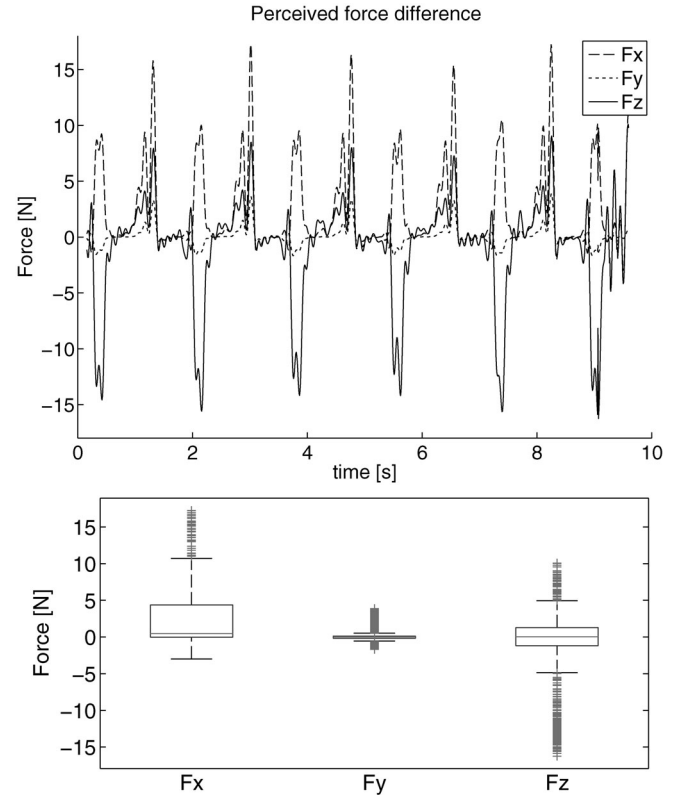


Fig. 17. Difference of forces due to oar inertia in outdoor rowing and on SPRINT.

## APPENDIX

### A. Oar Dynamics Effects

Dynamics effects that were not implemented are due to oar inertia and oar-water interaction. We took into account oars inertia and its effects on the system dynamics. We define  $I_{rG}$  the outdoor rowing oars inertia matrix referred to oar CoG and a coordinate system that has  $s$ -axis aligned with the oar shaft and  $n$ - and  $t$ -axes to compose a Cartesian right/handed frame. The inertia matrix for the SPRINTs oar referred to its center of rotation  $O$  and the same  $s$ ,  $n$ , and  $t$  axes is  $I_{sO}$ . Given oars angles we then have that the angular velocity and acceleration are

$$\omega_o = \begin{bmatrix} -\cos \varphi \dot{\alpha} \\ \dot{\varphi} \\ \sin \varphi \dot{\alpha} \end{bmatrix} \text{ and } \dot{\omega}_o = \begin{bmatrix} \sin \varphi \dot{\alpha} \dot{\varphi} - \cos \varphi \ddot{\alpha} \\ \ddot{\varphi} \\ \cos \varphi \dot{\alpha} \dot{\varphi} + \sin \varphi \ddot{\alpha} \end{bmatrix} \quad (33)$$

Then, we have that the force  $\mathbf{F}_o$  perceived due to rotational inertial effect is given by the equations

$$S(\mathbf{OHa})\mathbf{F}_o = (R_{y,\varphi} R_{x,\alpha})^T I_{sO} R_{y,\varphi} R_{x,\alpha} \dot{\omega}_o \text{ and} \quad (34)$$

$$S(\mathbf{GHa})\mathbf{F}_o = (R_{y,\varphi} R_{x,\alpha})^T I_{rG} R_{y,\varphi} R_{x,\alpha} \dot{\omega}_o \quad (35)$$

for the SPRINT oar and the outdoor rowing boat oar, respectively (see Appendix B for rotation matrices  $\mathbf{R}$  definition). Highest values of  $\mathbf{F}_o$  are obtained at highest speed (36–38 spm). Fig. 17 shows  $\mathbf{F}_o$  difference for the three components. The difference

between “real” and “SPRINT” perceived forces due to inertia  $F_o$  is always smaller than 5 N in the vertical component and 20 N in the horizontal components. Such result supports assumptions on oar inertia. During the blade immersion, the vertical force generated is negligible, drag force is generated by a small surface, and also skin force is small as the blade is almost flat. Bigger forces that may be generated on the shaft in fast and deep entry were not modeled.

### B. Rotation Matrices

Given a Cartesian frame  $(O,x,y,z)$  and given  $c_\delta$  and  $s_\delta$  the cosine and the sine of the angle  $\delta$  we define

$$R_{x,\delta} = \begin{bmatrix} 1 & 0 & 0 \\ 0 & c_\delta & -s_\delta \\ 0 & s_\delta & c_\delta \end{bmatrix}, R_{y,\delta} = \begin{bmatrix} c_\delta & 0 & s_\delta \\ 0 & 1 & 0 \\ -s_\delta & 0 & c_\delta \end{bmatrix} \text{ and}$$

$$R_{z,\delta} = \begin{bmatrix} c_\delta & -s_\delta & 0 \\ s_\delta & c_\delta & 0 \\ 0 & 0 & 1 \end{bmatrix}$$

the rotation matrices by  $\delta$  about axes  $x$ ,  $y$ , and  $z$ , respectively.

### ACKNOWLEDGMENT

The authors would like to thank Prof. M. Bergamasco, A. Frisoli, and C. A. Avizzano of PERCRO Lab. they would also like to thank to S. Marrucci, member of the staff of the Italian Rowing Federation, founder and coach of the Pontedera Rowing Club, and to this club’s guys for their advices and support.

### REFERENCES

- [1] E. Ruffaldi, A. Filippeschi, M. Varlet, C. Hoffmann, and B. Bardy, “Design, Evaluation of a multimodal VR Platform for Rowing training,” in *Skill Training in Multimodal Virtual Environments*. New York, NY, USA: Taylor & Francis, 2012.
- [2] A. Filippeschi, E. Ruffaldi, and M. Korman, “Preliminary evaluation of timing training accelerator for the SPRINT rowing system,” *BIO Web Conf.*, vol. 1, p. 25, 2011.
- [3] E. Ruffaldi and A. Filippeschi, “Structuring a virtual environment for sport training: A case study on rowing technique,” *Robot. Auton. Syst.*, vol. 61, no. 4, pp. 390–397, 2013.
- [4] C. P. Hoffmann, A. Filippeschi, E. Ruffaldi, S. Blanc, L. Verbrugge, and B. G. Bardy, “Mastering energy management during rowing using virtual reality,” *BIO Web Conf.*, vol. 1, p. 35, 2011.
- [5] A. Filippeschi, E. Ruffaldi, A. Frisoli, C. A. Avizzano, M. Varlet, L. Marin, J. Lagarde, B. Bardy, and M. Bergamasco, “Dynamic models of team rowing for a virtual environment rowing training system,” *Int. J. Virtual Reality*, vol. 4, no. 8, pp. 19–26, 2009.
- [6] R. A. Schmidt and T. D. Lee, *Motor Control and Learning: A Behavioral Emphasis*, 3rd ed. Champaign, IL, USA: Human Kinetics, 1999.
- [7] A. William *et al.*, in *Skill Acquisition in Sport*, J. N. Williams and A. Mark Hodges, Eds. Evanston, IL: Routledge, 2005.
- [8] J. Bailenson, K. Patel, A. Nielsen, R. Bajscy, S.-H. Jung, and G. Kurillo, “The effect of interactivity on learning physical actions in virtual reality,” *Media Psychol.*, vol. 11, no. 3, pp. 354–376, 2008.
- [9] K. M. Stanney, R. R. Mourant, and R. S. Kennedy, “Human factors issues in virtual environments: A review of the literature,” *Presence-Teleop Virtual*, vol. 7, no. 4, pp. 327–351, 1998.
- [10] (2006). *FISA Rowing Handbook*. FISA, [Online]. Available: <http://www.worldrowing.com/fisa/resources/>
- [11] E. T. Gjessing, “Friction type ergometer apparatus,” US Patent 4,047,715, Sep. 13, 1977.
- [12] B. Elliot, A. Lyttle, and O. Birkett, “The Rowperfect ergometer: A training aid for on-water single scull rowing,” *Sports Biomech.*, vol. 1, no. 2, pp. 123–134, 2007.
- [13] J. von Zitzewitz, P. Wolf, V. Novakovic, M. Wellner, G. Rauter, A. Brunschweiler, and R. Riener, “Real-time rowing simulator with multimodal feedback,” *Sports Technol.*, vol. 1, 2008.
- [14] V. Nolt *et al.*, in *Rowing Faster*, V. Nolte, Ed. Champaign, IL, USA: Human Kinetics, 2005.
- [15] F. H. Alexander, “The Theory of Rowing,” in *Proc. University of Durham Philosophical Society*, 1925, pp. 160–179.
- [16] M. Van Holst. (2011). “On Rowing,” [Online]. Available: <http://www.cyberiad.net/library/rowing/stroke/stroke.htm>
- [17] W. Atkinson. (2011). “Rowing computer research,” [Online]. Available: <http://www.atkinsopht.com/row/rowpage.htm>
- [18] A. Millward, “A study of the forces exerted by an oarsman and the effect on boat speed,” *J. Sport Sci.*, vol. 5, pp. 93–103, 1987.
- [19] L. Lazauskas. (1997). “A performance prediction model for rowing races,” University of Adelaide, Adelaide, Australia, Tech. Rep., [Online]. Available: <http://www.cyberiad.net/rowing.htm>
- [20] D. Cabrera, A. Ruina, and V. Kleshnev, “A simple 1+ dimensional model of rowing mimics observed forces and motions,” *Human Movement Sci.*, vol. 25, pp. 192–220, 2006.
- [21] A. Mola, “Multi.physics and multilevel fidelity modeling and analysis of olympic rowing boat dynamics,” Ph.D. dissertation, Virginia Polytechnic Institute and State University, Blacksburg, VA, USA, 2010.
- [22] V. Kleshnev, “Boat acceleration, temporal structure of the stroke cycle, and effectiveness in rowing,” *J. Sports Eng. Technol.*, vol. 224, no. 1, pp. 63–78, 2010.
- [23] A. Frisoli, E. Ruffaldi, L. Bagnoli, A. Filippeschi, C. A. Avizzano, F. Vanni, and M. Bergamasco, “Preliminary design of rowing simulator for in-door skill training,” presented at the Haptic in Ambient Systems, Quebec City, QC, Canada, 2008.
- [24] E. Ruffaldi, O. Gonzales, A. Filippeschi, A. Frisoli, C. A. Avizzano, and M. Bergamasco, “Integration of multimodal technologies for a rowing platform,” in *Proc. IEEE Int. Conf. Mechatron.*, 2009.
- [25] Y. Shorr, A. Filippeschi, D. Gopher, E. Ruffaldi, and M. Korman, “Evaluation of multimodal feedback effects on improving rowing competencies,” *BIO Web Conf.*, vol. 1, p. 83, 2011.
- [26] C. Cruz-Neira, D. J. Sandin, and T. A. DeFanti, “Surround-screen projection-based virtual reality: the design and implementation of the CAVE,” in *Proc. SIGGRAPH, Proc. 20th Annu. Conf. Comput. Graph. Interact. Techn.*, 1993, pp. 135–142.
- [27] E. Ruffaldi, A. Filippeschi, C. A. Avizzano, and M. Bergamasco, “Skill modeling and feedback design for training rowing with virtual environments,” in *Proceedings of 3rd Conference on Human Factors and Ergonomics*, 2010, D. Kaber and G. Boy, Eds., pp. 832–841.
- [28] E. Ruffaldi, “Data Management for evaluation and training in Virtual Environments,” in *Skill Training in Multimodal Virtual Environments*, D. B. Benoit and B. M. Gopher, Eds. New York, NY, USA: Taylor & Francis, 2012.
- [29] E. Ruffaldi, A. Filippeschi, C. Avizzano, B. Bardy, D. Gopher, and M. Bergamasco, “Feedback, affordances and accelerators for training sports in virtual environments,” *Presence-Teleop Virt.*, vol. 20, no. 1, Feb. 2011.
- [30] L. Formaggia, E. Miglio, A. Mola, and A. Montano, “A model for the dynamics of rowing boats,” *Int. J. Numer. Methods Fluids*, vol. 6, pp. 119–143, 2008.
- [31] “Skin Friction and Turbulence Stimulation,” in *Proc. 8th Int. Towing Tank Conf.*, 1957, pp. 71–227.
- [32] C. Scragg and B. Nelson, “The design of an eight-oared rowing shell,” *Marine Technol.*, vol. 30, no. 2, pp. 84–99, 1993.
- [33] E. O. Tuck, “The wave resistance formula of J.H. Michell (1898) and its significance to recent research in ship hydrodynamics,” *J. Austral. Math. Soc., Series B*, vol. 30, pp. 365–377, 1989.
- [34] R. L. Huston, in *Principles of Biomechanics*, C. Press and T. F. Group, Eds. Boca Raton, FL, USA: CRC Press, 2009.
- [35] V. Kleshnev. (2002). “Moving the rowers: Biomechanical background,” *Carine*, pp. 16–19, [Online]. Available: [http://www.biorow.com/Papers\\_files/2002MovingRowers.pdf](http://www.biorow.com/Papers_files/2002MovingRowers.pdf)
- [36] K. Hase, M. Kaya, N. Yamazaki, B. Andrews, Z. A. B., and S. Halliday, “Biomechanics of rowing,” *JSME Int. J. Series C Mech. Syst., Mach. Elements Manuf.*, vol. 45, no. 4, pp. 1073–1081, 2002.

Authors’ photographs and biographies not available at the time of publication.